Interplay between crystal electric field and magnetic exchange anisotropies in the heavy-fermion antiferromagnet YbRhSb under pressure

K. Umeo,[1,2,*] H. Yamane,[2] H. Kubo,[2] Y. Muro,[2,†] F. Nakamura,[2] T. Suzuki,[2] T. Takabatake,[2,3] K. Sengupta,[4,‡]
M. K. Forthaus,[4] and M. M. Abd-Elmeguid[4]

[1]*Cryogenics and Instrumental Analysis Division, N-BARD, Hiroshima University, Higashi-Hiroshima 739-8526, Japan*
[2]*Department of Quantum Matter, AdSM, Hiroshima University, Higashi-Hiroshima 739-8530, Japan*
[3]*Institute for Advanced Materials Research, Hiroshima University., Higashi-Hiroshima 739-8530, Japan*
[4]*II. Physikalisches Institut, Universität zu Köln, Zülpicher Str. 77, DE-50937 Köln, Germany*

We report the pressure effect on the magnetic ground state of the heavy-fermion (HF) canted antiferromagnet YbRhSb (orthorhombic ε-TiNiSi-type) by means of magnetization and resistivity measurements using a single crystal. At ambient pressure, this compound undergoes a transition at $T_{M1} = 2.7$ K into a canted antiferromagnetic (AF) state with a small spontaneous moment of 3×10^{-3} μ_B/Yb. With increasing pressure P above 1 GPa, another magnetic transition occurs at T_{M2} above T_{M1}, and $T_{M1}(P)$ has a deep minimum of 2.5 K at 1.7 GPa. For $P \geqslant 2$ GPa, the canted AF structure changes to a ferromagnetic (FM) one, where a large moment 0.4 μ_B/Yb lies in the orthorhombic b-c plane and a metamagnetic transition occurs at $B \parallel a = 1.5$ T. This unusual FM state below $T_{M3} \cong 4.3$ K is ascribed to the balance between the single-ion crystalline electric field (CEF) anisotropy with easy direction $\parallel a$ and the intersite exchange interaction with easy b-c plane. Furthermore, we have investigated the pressure dependence of T_{M3} up to 20.4 GPa using electrical resistivity measurements. The structural stability under pressures up to 19 GPa was examined by x-ray diffraction. We find that T_{M3} above 2.5 GPa steeply increases up to about 7 K, showing a broad maximum and then slightly decreases with increasing pressure above 8 GPa, while the structure remains unchanged. We attribute the enhancement of T_{M3} above 2.5 GPa to an increase of the CEF anisotropy with respect to magnetic exchange anisotropy. Finally, we compare and discuss the volume dependence of magnetic phase diagram of YbRhSb with the isostructural HF ferromagnet YbNiSn.

I. INTRODUCTION

In recent years, a considerable interest has been devoted to investigate Yb-based heavy-fermion (HF) systems as they exhibit many of the unusual ground-state properties found in Ce HF compounds.[1,2] Due to the hole-electron symmetry between the $4f^{13}$-Yb^{3+} and $4f^1$-Ce^{3+} configurations, these compounds offer an alternative and interesting way to investigate their physical properties close to a magnetic quantum critical point (QCP). Contrary to the Ce case, where the magnetic state is suppressed by pressure to a nonmagnetic state,[3,4] it is possible to drive a nonmagnetic Yb system into a magnetically ordered state under pressure and to follow the evolution of magnetism in the vicinity of the QCP. The nature of ground states in this class of compounds is mainly determined by competing onsite interaction via the Kondo effect and intersite Ruderman-Kittel-Kasuia-Yosida–(RKKY–)type magnetic interaction.[5,6] Therefore, one observes pressure-induced magnetism in nonmagnetic Yb compounds, e.g., Yb_2Ni_2Al,[7] $YbCu_2Si_2$,[8] and $YbPd_2Si_2$.[9] More interesting is the observation of complex phase diagrams associated with unusual ground states in Yb-based HF compounds located near a QCP, such as $YbRh_2Si_2$ ($T_N = 70$ mK) (Refs. [10,11]) and a frustrated antiferromagnet YbAgGe ($T_N = 0.8$ K).[12–14] In $YbRh_2Si_2$, one finds that the critical spin fluctuations associated with the low-moment state persist beyond the QCP up to a pressure of about 10 GPa, above which the system undergoes a first-order magnetic phase transition to a high-moment state with a high magnetically ordered temperature (T_M) of about 7.5 K.[10,11] A different pressure dependence of T_M has been observed in YbAgGe. Here, $T_M(P)$ remains

constant for $0.5 < P < P^* = 16$ GPa, while $T_M(P > P^*)$ increases linearly as P increases to 3.2 GPa.[12,13] The sudden increase in $T_M(P > P^*)$ was attributed to the partial release of the magnetic frustration in the quasi-kagome lattice.

Another interesting aspect of magnetically ordered HF systems is the existence of competing anisotropies of the magnetic exchange interaction and the crystalline electric field (CEF). This has been demonstrated in the ferromagnetic (FM) Kondo lattice compound YbNiSn.[15] The ground state of YbNiSn with an orthorhombic ε-TiNiSi-type structure changes from a FM state ($T_C = 5.6$ K) to a complex antiferromagnetic (AFM) state above 3 GPa.[15] This has been attributed to a volume-dependent competition between the anisotropy of the magnetic exchange interaction with easy direction $\parallel c$ and the CEF anisotropy with easy direction $\parallel a$.[15]

Recently, we have found that YbRhSb, being isostructural to YbNiSn but closer to a magnetic QCP, exhibits an anomalous P-T phase diagram.[16–18] At ambient pressure, this compound undergoes a transition at $T_M = 2.7$ K into an unusual magnetic state, which is associated with a very small spontaneous moment of 2–3×10^{-3} μ_B/Yb along all three principal directions.[19] A metamagnetic transition at 2.2 T in the isothermal magnetization process and the peaking of magnetic susceptibility at T_{M1} for $B \parallel b$ suggest that the weak ferromagnetism originates from a sort of canted AFM state.[19] Resistivity and ac magnetic susceptibility measurements under pressures revealed that another magnetic transition occurs at T_{M2} above T_{M1}, and $T_{M1}(P)$ has a deep minimum of 2 K at $P_C = 1.7$ GPa.[17,18] Furthermore, dc magnetization measurements under pressure showed that a FM state with net moments lying along the c axis is induced above

2 GPa.[17,18] Thus, the above-mentioned aspects of Yb-based HF compounds indicate that the complexity of the magnetic phase diagram and the nature of the high-pressure state strongly depend on the nature of the competing low-energy scales and, in particular, on the proximity of a specific system to a magnetic QCP.

In order to obtain a better understanding of the origin of the wide variety of the ground states in this class of materials, we have investigated the magnetic and electrical transport properties of single-crystal YbRhSb samples under pressures using dc magnetization and electrical resistivity measurements up to about 3 GPa. To compare the nature of the high-pressure state with that obtained for the isostructural compound YbNiSn, we have performed electrical resistivity measurements in an extended pressure range up to 20.4 GPa. In addition, high-pressure x-ray diffraction measurements up to 19 GPa were performed on YbRhSb to investigate the structural stability under high pressure.

II. EXPERIMENTAL DETAILS

Single crystalline samples of YbRhSb were grown by the Bridgeman method, as described previously.[19] The dc magnetization under pressures up to 2.5 GPa was measured with an indenter-type pressure cell made of Cu-Be alloy[20] and a piston-cylinder pressure cell made of NiCrAl alloy[21] by using a commercial superconducting quantum interference device magnetometer (Quantum Design) in magnetic fields (B) to 5 T at temperatures from 2 to 300 K. The electrical resistivity under pressures up to 3 GPa was measured by an ac four-terminal method using a piston-cylinder pressure cell in magnetic fields up to 9 T applied by a superconducting solenoid. Daphne oil was used as a pressure transmission medium in both pressure cells. The pressure was estimated from the pressure dependence of the superconducting transition temperatures of lead and/or tin. Measurements of the electrical resistance up to about 20 GPa between 1.5 and 300 K were performed in a diamond anvil cell (DAC) using a dc current four-point technique by measuring the voltage drop for both polarities. The DAC was made from a special Ti alloy, which ensures thermal stability against temperature variations. Thereby, the pressure gradient within the pressure cavity was about 5%–7%. Pressure was measured by the ruby luminescence method.[22,23] The lattice parameters as a function of pressure up to 19 GPa at 300 K were determined by energy-dispersive x-ray diffraction (EDXRD) at the Hamburger Synchrotronstrahlungslabor (HASYLAB) beam line F3 using the DAC technique. Liquid nitrogen was used as a pressure transmission medium. The pressure was determined by a gold marker in the sample chamber using the equation of state of the Au calibration standard.[24]

III. RESULTS AND DISCUSSIONS

A. Pressure dependence of T_M up to 3 GPa and change of the magnetic structure

Figure 1 presents isothermal magnetization curves $M(B)$ up to $B = 5$ T for $B \, || \, a$, $B \, || \, b$, and $B \, || \, c$ at 2 K under pressures up to 2.5 GPa. With increasing pressure, the magnitude of M for all axes increases. For $B \, || \, a$, metamagnetic anomalies
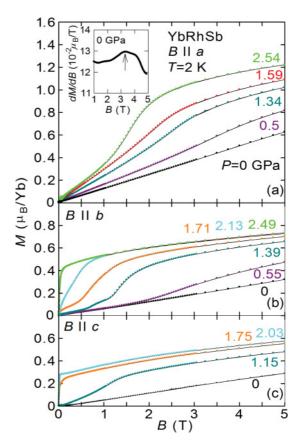

FIG. 1. (Color online) Isothermal magnetization curves $M(B)$ of YbRhSb for $B \, || \, a$, $B \, || \, b$, and $B \, || \, c$ at 2 K under pressures up to 2.5 GPa. The inset shows the field derivative of $M(B)$ for $B \, || \, a$ at $P = 0$.

are observed at 3.2 T for $P = 0$ as shown in the inset, which become clearer and shifts to 1.5 T at 2.5 GPa. However, the magnetization curves for $B \, || \, b$ at 2.49 GPa and $B \, || \, c$ above 1.75 GPa exhibit a definite FM behavior with remanent moments of 0.4 μ_B/Yb and 0.3 μ_B/Yb, respectively.

The temperature dependence of the magnetic susceptibility $\chi = M/B$ along the b axis under various pressures is shown in Fig. 2. With increasing pressure, the upturn of χ at T_{M1} shifts to a higher temperature. Above 1.3 GPa, however, the upturn at T_{M1} shifts to a lower temperature. A broad maximum, which is a manifestation of an AFM order, appears at $T_{M2} = 3.5$ K. This maximum is consistent with the anomaly at T_{M2} in the ac susceptibility.[16] With further increasing pressure, the upturn at T_{M1} grows to a steep increase at T_{M3} and shifts to a higher temperature. This implies the enhancement of the FM component in consistentcy with the development of the FM state above 2 GPa as shown in Fig. 1.

Figure 3 shows the temperature dependence of the inverse magnetic susceptibilities B/M of YbRhSb for $B \, || \, a$, $B \, || \, b$, and $B \, || \, c$ under pressures up to 2.5 GPa. Above 150 K, all data sets follow the Curie-Weiss law with the effective magnetic moments, the values of which are almost constant 4.2 ∼ 4.4 μ_B/Yb. Thus, the valence of Yb hardly changes in this pressure range. The paramagnetic Curie temperatures θ_p at $P = 0$ are −47, −95, and −145 K for $B \, || \, a$, $B \, || \, b$, and $B \, || \, c$, which are close to the previous data.[19]
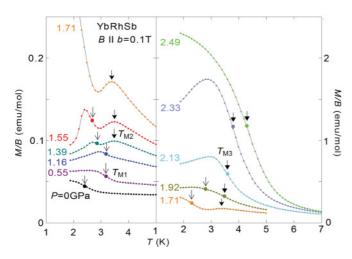
FIG. 2. (Color online) Temperature dependence of the magnetic susceptibility M/B of YbRhSb for $B \parallel b$ under pressures up to 2.5 GPa. Arrows indicate transition temperatures.

The pressure dependence of θ_p for the three axes is plotted in Fig. 4(b), which is compared with that of the magnetic ordering temperatures in Fig. 4(a).[18] For a FM order, the temperature at the negative peak of $d\chi/dT$ gives the ordering temperature, which in fact agrees with the temperature T_{M3} at the midpoint of the jump of $C(T)$.[18] The decrease of $\theta_P(P)/\theta_P(0)$ for all axes suggests the decrease of Kondo temperature T_K.[25] It is noteworthy that above 2 GPa, $T_{M3}(P)$ increases sharply, but all of θ_p are almost constant. This fact suggests that the increment of T_{M3} is not due to the suppression of Kondo interaction but the enhancement of RKKY interaction.

Figure 4(b) clearly shows that the relative decrease of θ_p along the a axis is about a factor of 3 larger than those along b and c. Since the anisotropy of θ_p in related rare-earth $R\mathrm{Cu}_2$ intermetallic compounds[26] is mainly determined by the corresponding anisotropy of CEF, these results strongly suggest an increase of the CEF anisotropy with pressure along the a axis. As we will show in Sec. III B, such an anisotropic magnetic behavior is associated with a corresponding anisotropic change of the lattice parameters with pressure.
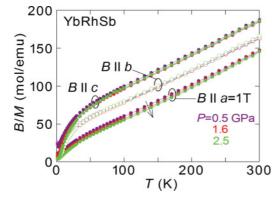

FIG. 3. (Color online) Temperature dependence of the inverse magnetic susceptibility B/M of YbRhSb measured at $B = 1$ T applied along the a, b, and c axes under pressures at 0.5, 1.6, and 2.5 GPa.
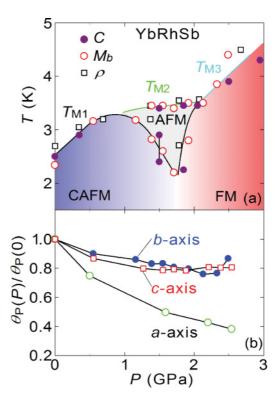

FIG. 4. (Color online) (a) P-T phase diagram of YbRhSb in the low-pressure range up to 3 GPa from Ref. 18. (b) Pressure dependence of the normalized value $\theta_P(P)/\theta_P(0)$ of the paramagnetic Curie temperature θ_P for $B \parallel a$, $B \parallel b$, and $B \parallel c$.

We now focus on the pressure dependence of magnetic structure of YbRhSb. Our magnetization measurements combined with recent Sb nuclear magnetic resonance (NMR) measurements[27] suggested that the magnetic moments are lying along the b axis below T_{M1} at ambient pressure. Between 1 and 2 GPa, an AFM state is realized below T_{M2} as referred from the peak in M/B versus T in Fig. 3. This AFM state is suppressed by applying magnetic fields as shown in Figs. 5(a) and 5(b). In a higher-pressure region $2 < P < 2.5$ GPa, a FM ground state appears with a spontaneous moment of $0.3 \mu_B$/Yb, which probably orients along the c axis. However, a metamagnetic behavior for $B \parallel a$ remains even in the FM state [see Fig. 1(a)]. These facts are consistent with the field dependences of $\rho(B)$ in Figs. 5(c) and 5(d), where T_{M3} at 2.07 GPa decreases by applying field for $B \parallel a$ while it increases for $B \parallel c$. Above 2.5 GPa, the FM moments most likely lie in the b-c plane. A similar metamagnetic behavior along the a axis was reported in the isostructural compound YbNiSn, while the ground state has a collinear FM structure with moments parallel to the c axis.[28] This unusual situation in YbNiSn was attributed to the competition between the strong anisotropic exchange interaction with the easy direction along the c axis and the CEF anisotropy with the easy a axis. As shown in Fig. 3, the CEF anisotropy of YbRhSb with easy a axis in the paramagnetic state hardly changes under pressures up to 2.5 GPa, keeping the a axis as the easy direction. Furthermore, the Kondo temperature T_K also hardly changes above 1.5 GPa. Therefore, the complicated pressure-induced magnetic state of YbRhSb is attributed to the enhancement of intersite exchange interaction in the easy b-c plane. For direct
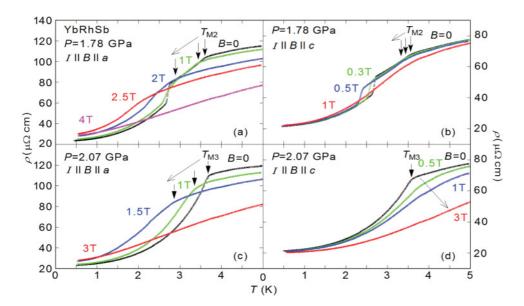
FIG. 5. (Color online) Temperature dependence of electrical resistivity ρ of YbRhSb in various magnetic fields for the longitudinal configurations I || B || a and I || B || c at $P = 1.78$ and 2.07 GPa.

determination of the detailed magnetic structures, neutron diffraction and NMR measurements under pressure are highly desired.

B. Magnetic phase diagram up to 20.4 GPa and comparison with YbNiSn

Figure 6 displays the results of $\rho(T, P)$ of YbRhSb between 1.5 and 300 K at different pressures up to 20.4 GPa. For a better comparison, the curves are normalized to the value at 290 K. As it is evident from Fig. 6, $\rho(T, P)$ shows a double-maximum structure as reported in related Yb compounds such as YbNiSn,[29] Yb_2Ni_2Al,[5] and $YbRh_2Si_2$.[8] The broad maximum at high temperatures, $T_{CEF} = 107$ K at ambient pressure, is suggested to be due to an incoherent scattering of the conduction electrons at the first excited CEF level. This assumption is strongly supported by inelastic neutron scattering data and high-temperature resistivity data of the related isostructural ferromagnetic Kondo lattice compounds, e.g., YbNiSn (Refs. 30 and 31) and YbPtGa.[32,33] Here, it has been shown that the first excited CEF levels are located at 12.3 (Ref. 30) and 13 meV,[31] respectively, which correspond

to about 140 and 150 K. As these compounds reveal broad maxima in the high-temperature resistivity around 100 K,[31,33] it is most likely to assume similar first excited CEF state in YbRhSb, which causes the observed broad maximum observed at about 107 K. As it shown in the inset of Fig. 6, the broad maximum at T_{CEF} gradually increases with pressure. This behavior is qualitatively similar to that observed in YbNiSn,[29] which reflects an increase of the characteristic energy of CEF effects with increasing pressure.

At low temperatures below about 15 K, the resistivity develops a shoulder that is followed by a sharp drop at lower temperatures due to the onset of magnetic order. Figure 7(a) displays the low-temperature part of the resistivity
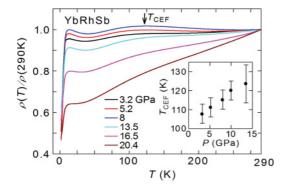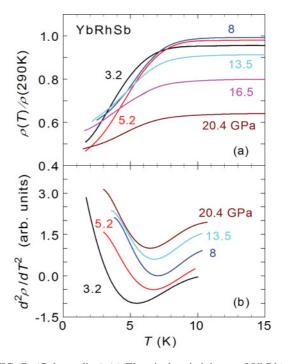

FIG. 6. (Color online) Temperature dependence of electrical resistivity ρ of YbRhSb normalized at 290 K under various constant pressures up to 20.4 GPa. The inset shows the pressure dependence of T_{CEF} up to 13.5 GPa since the values of T_{CEF} at higher pressures are ambiguous.

FIG. 7. (Color online) (a) Electrical resistivity ρ of YbRhSb in the temperature range between 1.5 and 15 K at different pressures. (b) Second derivatives of $\rho(T)$ curves for different pressures.
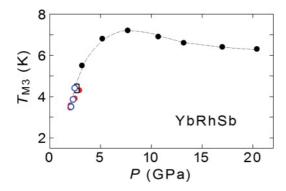
FIG. 8. (Color online) Pressure dependence of the ordering temperature in the ferromagnetic state (T_{M3}) as deduced from Fig. 7(b). The values of T_{M3} in the low-pressure range [see Fig. 4(a)] are also included.

at some selected pressures. We have deduced the magnetic ordering temperature T_{M3} from the minimum in the second derivative of $d^2\rho/dT^2$, which is shown in Fig. 7(b). The obtained values of T_{M3} at different pressures are plotted in Fig. 8 together with the values of T_{M3} in the lower pressure range up to about 3 GPa [see Fig. 4(a)]. T_{M3} steeply increases up about 7 K, showing a broad maximum, and then slightly decreases with increasing pressure above 8 GPa.

To clarify whether the observed anomalous behavior of T_{M3} for YbRhSb is connected with structural instabilities, we consider the pressure effect on the structural parameters as obtained from our EDXRD measurements up to 19 GPa. The pressure dependence of the lattice parameters and the unit-cell volume are presented in Fig. 9. We obtain a smooth variation of the lattice parameters (a, b, and c) and the volume, which exclude any structural changes up to 19 GPa. A fit to the data using Birch's equation of state results in values of a bulk modulus $B_0 = 114(9)$ GPa and its pressure derivative $dB_0/dP = 5(1)$.[34] The value of B_0 is lower than that obtained for YbNiSn [$B_0 = 146(20)$ GPa].[29] In addition, we find an anisotropic change of the lattice parameters with pressure: the values of the inverse of the linear compressibility are $B_0(a) = 32(2)$ GPa, $B_0(b) = 53(3)$ GPa, and $B_0(c) = 77(3)$ GPa along the a, b, and c axes, respectively. This indicates a much higher compression along the a axis with respect to the b and c axes that correlates with the observed anisotropy of θ_p shown in Fig. 4(b).

Using the obtained equation of state, one can compare the magnetic phase diagram of YbRhSn in the (T, P) space with that known for the isostructural-related HF ferromagnet Yb-NiSn. This is shown in Fig. 10, in which we plot the variation of T_M with decreasing the unit-cell volume. We note that at ambient pressure, the unit-cell volume of YbRhSb (244 Å^3) is larger than that of YbNiSn (233.5 Å^3) and thereby reflects the proximity of YbRhSb to a magnetic QCP. This in turn causes the complexity of the pressure dependence of T_M for YbRhSb in the low-pressure range up to about 3 GPa, as we discussed in Sec. III A. At higher pressures, however, we find that T_{M3} for YbRhSb exhibits qualitatively similar pressure dependence as the Curie temperature (T_C) of YbNiSn. As shown in Fig. 10, both temperatures T_{M3} and T_C increase to a maximum and then decrease. Also, we note that maximum values of T_{M3}
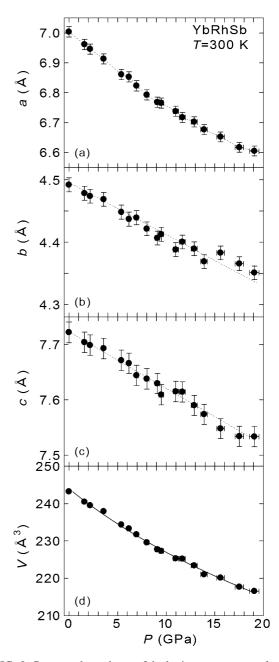

FIG. 9. Pressure dependence of the lattice parameters a, b, c, and unit-cell volume of YbRhSb at 300 K as deduced from the analysis of the energy-dispersive x-ray diffraction patterns. Dotted lines through the data points are only a guide to the eyes. The solid line through the data points of $V(P)$ is a fit using Birch's equation of state.

and T_C occur nearly around the same value of the unit-cell volume.

The reason of such a similarity can be understood in terms of the common nature of the pressure-induced FM state in YbRhSb and FM state in YbNiSn at ambient pressure and the associated competition between the anisotropic magnetic exchange interactions and the CEF anisotropy. According to our discussion in Sec. III A, we find above 2.5 GPa a pressure-induced FM state, the nature of which is governed by the balance between the strong anisotropic exchange interaction with the easy direction along the c axis and the CEF anisotropy with the easy a axis. We note that the observed increase of
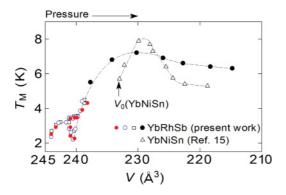
FIG. 10. (Color online) Magnetic phase diagram of YbRhSb up to 20.4 GPa and comparison with that of YbNiSn using the equation of state of both compounds. The volume dependence of the ordering temperatures in the different phases in the low-pressure range up to 3 GPa is included. The experimental data points for the HF ferromagnet YbNiSn are reproduced from Refs. 15 and 29 using the equation of state.

T_{CEF} with pressure implies an increase of the energy of the CEF anisotropy, which is in turn connected with higher compressibility along the *a* axis. This finding is consistent with the observed anisotropic large decrease of θ_p along the *a* axis [see Fig. 4(b)].

The same competing energy scales are also responsible for the unusual FM state of YbNiSn at ambient pressure.[15] Since the observed anomalous behavior of T_C in YbNiSn under pressure has been shown to be connected with an increase in the CEF anisotropy with respect to the anisotropy of the magnetic exchange interaction,[15,29] one expects similar pressure dependence of the ferromagnetic ordering temperatures in the two systems (see Fig. 10). However, the question remains to be answered as to why the pressure dependence of T_{M3} in the FM state of YbRhSb up to highest pressure is weaker than that of YbNiSn, in particular, the broader maximum of $T_{M3}(P)$ in YbRhSb. A possible explanation could be that the relative strength of CEF anisotropy with respect to the anisotropy of the exchange interaction is different between the two systems.

IV. SUMMARY

We have studied the effect of pressure on the magnetic ground state of YbRhSb (orthorhombic ε-TiNiSi-type structure), which undergoes at ambient pressure a transition at $T_{M1} = 2.7$ K into a canted AFM state with a small spontaneous moment of 3×10^{-3} μ_B/Yb. Our high-pressure experiments up to about 3 GPa on single-crystal samples using dc magnetization and resistivity measurements showed a complex magnetic behavior. We found above 1 GPa another magnetic transition at a higher temperature ($T_{M2} \sim 3.2$ K) and, for $P \geqslant 2$ GPa, a pressure-induced change to a FM state with a large moment 0.4 μ_B/Yb ($T_{M3} \sim 4.3$ K) lying in the orthorhombic *b-c* plane. This unusual magnetic behavior is explained by a pressure-dependent competition between the single-ion CEF anisotropy with easy direction $\| a$ and the intersite exchange interaction with easy *b-c* plane. The pressure dependence of the ordering temperature T_{M3} of the FM state has been further investigated up to about 20 GPa using electrical resistivity measurements. We found that for $P > 2.5$ GPa, T_{M3} rapidly increases to about 7 K, going through a broad maximum, and then slightly decreases with increasing pressure above 8 GPa. No structural change up to 19 GPa was observed by x-ray diffraction measurements at room temperature. Therefore, the enhancement of T_{M3} for $P > 2.5$ GPa is attributed to an increase of the CEF anisotropy with respect to magnetic exchange anisotropy. The obtained magnetic phase diagram of YbRhSb as a function of the unit-cell volume has been discussed and compared with that of the isostructural HF ferromagnet YbNiSn.

*kumeo@sci.hiroshima-u.ac.jp

†Present address: Liberal Arts and Sciences, Faculty of Engineering, Toyama Prefectural Univ., Imizu-shi, Toyama, 939-0398, Japan.

‡Present address: Saha Institute of Nuclear Physics, 1/AF Bidhannagar, Kolkata 700064, India.

[1]R. Movshovich, A. Lacerda, P. C. Canfield, J. D. Thompson, and Z. Fisk, Phys. Rev. Lett. **73**, 492 (1994).

[2]S. Nakatsuji, K. Kuga, Y. Machida, T. Tayama, T. Sakakibara, Y. Karaki, H. Ishimoto, S. Yonezawa, Y. Maeno, E. Pearson, G. G. Lonzarich, L. Balicas, H. Lee, and Z. Fisk, Nat. Phys. **4**, 603 (2008), and references therein.

[3]K. Umeo, H. Kadomatsu, and T. Takabatake, J. Phys.: Condens. Matter **8**, 9743 (1996).

[4]G. R. Stewart, Rev. Mod. Phys. **73**, 797 (2001).

[5]S. Doniach, Physica B+C (Amsterdam) **91**, 231 (1977).

[6]J. D. Thompson and J. L. Lawrence, in *Handbook on the Physics and Chemistry of Rare Earths*, edited by K. A. Gschneidner Jr., L. Eyring, G. H. Lander, and C. Choppin (North-Holland, Amsterdam, 1994), Vol. 19, p. 383.

[7]H. Winkelmann, M. M. Abd-Elmeguid, H. Micklitz, J. P. Sanchez, C. Geibel, and F. Steglich, Phys. Rev. Lett. **81**, 4947 (1998).

[8]H. Winkelmann, M. M. Abd-Elmeguid, H. Micklitz, J. P. Sanchez, P. Vulliet, K. Alami-Yadri, and D. Jaccard, Phys. Rev. B **60**, 3324 (1999).

[9]T. Nakano, M. Hedo, Y. Uwatoko, and E. V. Sampathkumaran, Solid State Commun. **132**, 325 (2004).

[10]J. Plessel, M. M. Abd-Elmeguid, J. P. Sanchez, G. Knebel, C. Geibel, O. Trovarelli, and F. Steglich, Phys. Rev. B **67**, 180403 (2003).

[11]G. Knebel, R. Boursier, E. Hassinger, G. Lapertot, P. G. Niklowitz, A. Pourret, B. Salce, J. P. Sanchez, I. Sheikin, P. Bonville, H. Harima, and J. Flouquet, J. Phys. Soc. Jpn. **75**, 114709 (2006).

[12]K. Umeo, K. Yamane, Y. Muro, K. Katoh, Y. Niide, A. Ochiai, and T. Takabatake, Phys. B (Amsterdam) **359-361**, 130 (2005).

[13]H. Kubo, K. Umeo, K. Katoh, A. Ochiai, and T. Takabatake, J. Phys. Soc. Jpn. **77**, 023704 (2008).

[14]K. Sengupta, M. K. Forthaus, H. Kubo, K. Katoh, K. Umeo, T. Takabatake, and M. M. Abd-Elmeguid, Phys. Rev. B **81**, 125129 (2010).

[15]K. Drescher, M. M. Abd-Elmeguid, H. Micklitz, and J. P. Sanchez, Phys. Rev. Lett. **77**, 3228 (1996).

[16]K. Umeo, H. Kubo, F. Nakamura, Y. Haizaki, K. Katoh, A. Ochiai, and T. Takabatake, J. Phys. Soc. Jpn. **76**, 74 (2007).

[17]K. Umeo, H. Kubo, Y. Muro, F. Nakamura, T. Suzuki, and T. Takabatake, J. Phys.: Conf. Ser. **150**, 042223 (2009).

[18]K. Umeo, H. Yamane, H. Kubo, Y. Muro, and T. Takabatake, J. Phys.: Conf. Ser. **200**, 012215 (2010).

[19]Y. Muro, Y. Haizaki, M. S. Kim, K. Umeo, H. Tou, M. Sera, and T. Takabatake, Phys. Rev. B **69**, 020401(R) (2004).

[20]T. C. Kobayashi, H. Hidaka, H. Kotegawa, K. Fujiwara, and M. I. Eremets, Rev. Sci. Instrum. **78**, 023909 (2007).

[21]R. Nakai, F. Nakamura, and T. Suzuki, J. Phys. Soc. Jpn. **76**, 219 (2007).

[22]G. J. Piermarini, S. Block, J. D. Barnett, and R. A. Forman, J. Appl. Phys. **46**, 2774 (1975).

[23]H. K. Mao, J. Xu, and P. M. Bell, J. Geophys. Res. **91**, 4673 (1986).

[24]D. L. Heinz and R. Jeanloz, J. Appl. Phys. **55**, 885 (1984).

[25]G. Grüner and A. Zawadowski, Rep. Prog. Phys. **37**, 1497 (1974).

[26]Y. Hashimoto, H. Fujii, H. Fujiwara, and T. Okamoto, J. Phys. Soc. Jpn. **47**, 67 (1979).

[27]H. Tou (private communications).

[28]M. Kasaya, T. Tani, K. Kawate, T. Mizushima, Y. Isikawa, and K. Sato, J. Phys. Soc. Jpn. **60**, 3145 (1991).

[29]K. Drescher, M. M. Abd-Elmeguid, J. P. Sanchez, and C. Meyer, J. Phys.: Condens. Matter **8**, L65 (1996).

[30]M. Kasaya, T. Tani, F. Iga, and T. Kasuya, J. Magn. Magn. Mater. **76-77**, 278 (1988).

[31]D. T. Adroja, B. D. Rainford, and T. Takabatake, Phys. B (Amsterdam) **253**, 269 (1998).

[32]D. T. Adroja, B. D. Rainford, L. E. Miller, and S. K. Malik, Phys. B (Amsterdam) **230-232**, 282 (1997).

[33]Y. Itoh and H. Kadomatsu, J. Alloys Compd. **280**, 39 (1998).

[34]F. Birch, Phys. Rev. **71**, 809 (1947).